

A Machine Learning Approach for Material Type Logging and Chemical Assaying from Autonomous Measure-While-Drilling (MWD) Data

Rami N. Khushaba · Arman Melkumyan ·
Andrew J. Hill

Received: Dec 2020 / Accepted: date

Abstract Understanding the structure and mineralogical composition of a region is an essential step in mining, both during exploration (before mining) and in the mining process. During exploration, sparse but high-quality data is gathered to assess the overall orebody. During the mining process, boundary positions and material properties are refined as the mine progresses. This refinement is facilitated through drilling, material logging, and chemical assaying. Material type logging suffers from a high degree of variability due to factors such as the diversity in mineralization and geology, the subjective nature of human-measurement even by experts, and human errors in manually recording results. While laboratory-based chemical assaying is much more precise, it is time-consuming and costly and does not always capture or correlate boundary positions between all material types. This leads to significant challenges and financial implications for the industry, as the accuracy of production blast-hole logging and assaying processes is essential for resource evaluation, planning and execution of mine plans.

To overcome these challenges, this work reports on a pilot study to automate the process of material logging and chemical assaying. A machine learning approach has been trained on features extracted from measure-while-drilling (MWD) data, logged from autonomous drilling systems (ADS). MWD data facilitates building profiles of physical drilling parameters as a function of hole depth. A hypothesis is formed to link these drilling parameters to the underlying mineral composition. The pilot study results in this paper demonstrate the feasibility of this process, with correlation coefficients of up to 0.92 for chemical assays and 93% accuracy for materials detection, depending on the material or assay type and their generalization across the different

All authors are within the Rio Tinto Centre for Mine Automation, Australian Centre for Field Robotics, The University of Sydney
8 Little Queen street, Chippendale, NSW 2008.
Tel.: +61 2 9351 4209
E-mail: Rami.Khushaba@sydney.edu.au,
Arman.Melkumyan@sydney.edu.au,
Andrew.Hill@sydney.edu.au
Corresponding author ORCID: <https://orcid.org/0000-0001-8528-8979>

spatial regions. The achieved results are significant, showing opportunities to guide further drilling processes, provide chemistry data with a down-hole resolution, and continuously update mine plans as the mine progresses.

Keywords mining · measure-while-drilling · logging and assaying · machine learning

1 Introduction

The mining industry has embarked on a journey to use automation to improve the accuracy and consistency of mining processes within its surface mines. Blast-hole drilling is a key task in most surface mining, as the accuracy of the information obtained affects the entire downstream mining process. This has impacts on i) scheduling, ii) excavation, iii) slope stability, iv) material handling, v) beneficiation, vi) ore loss and vii) final product blending (McHugh et al. 2012). Measurement-while-drilling (MWD) enables the collection of accurate, fast and high-resolution information from production blast-hole drills for equipment automation and monitoring the health of major drilling items (Rai et al. 2015). In open-pit mining, MWD systems monitor several performance factors including, but not limited to, i) rate of penetration, ii) torque, iii) rotation pressure, iv) specific energy of drilling, v) weight on bit and vi) rotary speed. These factors are becoming standard features on the blast-hole drill rigs supplied by most equipment manufacturers (Hatherly et al. 2015). MWD data has already been utilized in applications related to i) rock type recognition (Zhou et al. 2010), ii) boundary identification and surface updates (Siversides and Melkumyan 2020), iii) automated coal seam detection (Leung and Scheduling 2015), iv) estimation of rock mass rating during tunneling (Galende et al. 2018), v) rock fracture density characterization (Khorzoughi et al. 2018), vi) improving rock-breakage efficiencies (Park and Kim 2020), vii) developing a prediction model of over- and under-excavation depths from blasting (Navarro et al. 2018), viii) characterizing a coal mine roof (Khanal et al. 2020), and ix) identifying the top of coal seams allowing drilling to be halted to prevent unintended blasting of coal and associated problems (Hatherly et al. 2015). However, an extensive literature review has not uncovered any use of MWD data to estimate material types or chemistry assays.

Boreholes and blast-holes are routinely logged and assayed to assist in the understanding of the structures and mineralogical compositions of an area (Sommerville et al. 2014), the accuracy of which is essential for resource evaluation and planning in the minerals industry. Material logging is the process of recording manual geological observations to identify the material types present in the sample, and chemistry assaying is generally a lab-based process to quantify the chemical make-up of samples (valuable minerals, impurities and water content).

To standardize primary characteristics, such as mineralogy and texture, in a hierarchical manner, the Material Type Classification Scheme was developed (Box et al. 2002; Wedge et al. 2019). This scheme models physical and chemical attributes for predicting metallurgical behavior and the quality of the product for optimal ore processing (Paine et al. 2016). Logging of material-types is usually performed on chip

samples produced by reverse circulation (RC) drills during exploration (in 2m intervals) or blast-hole cone samples (one sample per blast hole). This generates a huge number of samples and significant costs and time in preparation and assaying. For each sample, a geologist manually handles the material and estimates several parameters including (Sommerville et al. 2014; Wedge et al. 2018): (i) the percentages of various material types present in the sieve (usually in increments of 5%), (ii) the sample color, (iii) the shape of the chips, and (iv) the percentage of material recovered. Another sample is usually sent for laboratory X-ray fluorescence assay analysis to measure i) aluminium oxide (Al_2O_3), ii) iron (Fe), iii) silicon dioxide (SiO_2), iv) phosphorus (P), v) sulfur (S), vi) manganese (Mn), vii) magnesium oxide (MgO), viii) titanium dioxide (TiO_2), ix) calcium oxide (CaO), and x) total loss on ignition (LOI). However, this approach has limitations as exploration holes are sparse in the horizontal direction, while horizontally denser blast-holes provide only a single sample for the entire hole (e.g. 10-15m depth). For these reasons, the literature criticizes assaying from RC boreholes or blast-hole samples in that they do not always provide truly representative analysis (Clark and Dominy 2017), are not always effective at characterizing thin layers, and the sampling is costly to perform. As a result, there has been an increased interest in downhole, in-situ assaying. Downhole Pulsed Fast and Thermal Neutron Activation (PFTNA) has been proven through its operations to date to provide a downhole in-situ assaying technique that has several advantages over conventional sample-based assays in terms of safety, cost, cycle-time of results, and accuracy (Jeanneau et al. 2017; Market et al. 2019). By removing the need for manual samples taken on-site, tools relying on PFTNA technology limit the exposure of workers to manual handling, operational and environmental safety risks typical on many mine sites.

It is important to mention here that the use of PFTNA-based technologies alone does not completely obviate the need for manual handling for logging purposes, as such technologies are primarily used for assaying, while material logging is not facilitated by PFTNA. It has been reported that using PFTNA for in-situ measurements, as an alternative to traditional chemical analysis, may be overly-simplistic, as it does not provide some vital information such as hardness (Smith et al. 2015). Additionally, PFTNA does not produce estimation for all assays, especially trace elements which can be of particular importance in some deposits, such as P in iron ore, or Au and Ag in copper.

This paper argues that improvements in drilling technology can change the way mineral deposits are observed. The motivation of this work is driven by the fact that MWD data has already been deemed useful for several applications (Zhou et al. 2010; Silversides and Melkumyan 2020; Leung and Scheduling 2015; Galende et al. 2018; Khorzoughi et al. 2018; Park and Kim 2020; Navarro et al. 2018; Khanal et al. 2020; Hatherly et al. 2015), which lends itself as a potential tool for determining the material-types and chemical assays. Hence, the primary hypothesis of this work is that using MWD and machine learning can help predict chemical assays and materials. This is a novel application of MWD data, which has not been previously verified and is based on a common conclusion that the drilling behavior is related to the mechanical properties of the material being drilled. The result would be a downhole in-situ assaying or logging “equipment-as-a-sensor” tool that lends itself particularly

well to bulk mining operations such as that found in the iron ore operations in the Pilbara¹. Additionally, MWD data has good down-hole resolution and can be made available in real-time, during drilling. A key challenge is the difficulty modelling the bit–rock interaction because of high-order variability in different rocks or even simply at different sample points in the same rock material due to the presence of cracks, fissures and a host of other discontinuities (Rai et al. 2015). This is where the use of machine learning (ML) models to capture the relation between the MWD data and materials or assays become increasingly important. The application of ML in this problem is supported by wide-ranging successes of using ML in several applications in the era of big data (L’Heureux et al. 2017).

2 Data Sources

This pilot study was conducted on an Iron Ore mine site in the Hammersley Range, which is located in the Pilbara region of Western Australia. MWD, material logging and chemistry assay data was collected from two physically separate regions, labelled here as Regions A and B.

2.1 MWD Data

MWD data represents real-time measurements of several mechanical signals, collected from sensors equipped on relatively large drill-rigs used in mining for blast-hole drilling. These signals are commonly used to control and monitor the performance of drilling. Fig. 1 shows the autonomous blast-hole drill rig that collects the MWD data used in this paper. The parameters of interest considered in this paper include: i) the time taken for hole development (start to finish), ii) measurement depth, iii) average head rotation speed (rotationRPM), iv) average bit air pressure (airPressure), v) average feed pressure (feedPressure), vi) average torque (torque), vii) average rate of penetration (rop), viii) average force on bit (fob), ix) average rotation pressure (rotationPressure), x) adjusted penetration rate (apr), and xi) specific energy of drilling (sed). Also considered is the ratio of rotationPressure to feedPressure as another parameter. The MWD time-series data were logged by the drilling system as discretized sequences, typically discretised into depth segments of 0.1 meter resolution (Hatherly et al. 2015). A total of almost 7000 holes’ data were logged by the ADS system, as MWD is available for every hole. This is not the case for materials/assays data as mentioned in the next section.

2.2 Logging and Assaying

The logged material-types and chemistry assay data were provided from multiple blasts within both Region A and Region B. While the autonomous drilling system

¹ <https://en.wikipedia.org/wiki/Pilbara>



Fig. 1 Autonomous blast-hole drill rig used for collecting experimental MWD data

provided MWD data along the full depth of every blast-hole, the data for material-types and chemistry is only available for a subset of the holes, and where available is a single value per hole for each material and chemistry parameter (depicted in Fig.2). This is primarily due to the cost of data collection, including manual logging, manual physical sampling and laboratory analysis costs. Additionally, this data is delayed by the collection and analysis time, while MWD data is collected electronically and is immediately available after drilling.

The resulting data set comprises MWD for all holes, and subsets of holes that also include material logging and/or chemistry assays, as noted in Table 1.

Additionally, wherever material logging is available, a theoretical chemistry assay is also estimated by geologists. A validation process is usually performed by geologists after logging, adjusting the percentages of the logged material types or adding/removing material types where necessary, using geologically informed substitutions so that the theoretical assay values are within an error tolerance of the laboratory assay values obtained from the interval's chip samples (Wedge et al. 2018).

Data Sources	Region A	Region B	Total
MWD + Material	805	993	1,798
MWD + Chemistry	2,176	2,408	4,584
MWD + Mat. + Chem.	537	804	1,341

Table 1 Material logging and chemistry assays are collected more sparsely than MWD data, resulting in multiple subsets of holes with different combinations of data for the same hole

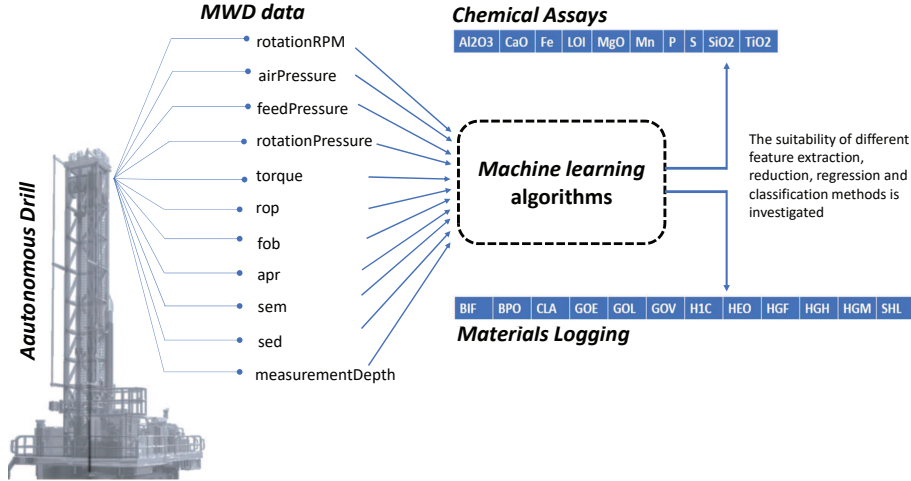


Fig. 2 The three sources of data available for this pilot study. MWD is sampled at 0.1m intervals across the entire hole depth, while assay and material types offer a single value per hole for each parameter, for the subset of holes where they are collected

3 Details of the Machine Learning Pipeline

3.1 Feature Extraction

The literature review showed that there is no generally agreed-upon quantitative method for the description of the MWD data. As such, several feature extraction methods are investigated in detail in this study. As our hypothesis attempts to relate the changes in the drilling parameters to the changes in materials and chemical assays underground, we have sought features focusing on changes in the amplitude, energy, complexity, frequency contents and shape of the power spectrum, signals' peak values, root mean square and entropy of the signals to denote the dispersion. The selected methods have been utilized across different time-series data in other domains, demonstrating significant success in describing signals (Hjorth 1970; Khushaba et al. 2014; Phinyomark et al. 2010), and hence are seen as good candidates to employ to describe the MWD signals. The investigated feature extraction methods are described below. In the following features' descriptions, we assume a signal \mathbf{x} , with $x[j]$ representing its j -th sample, where $j = 0, 2, 3, \dots, N - 1$, with a length of N samples.

Hjorth parameters:

These parameters were originally developed in an approach to describe the shape of the frequency spectrum of any signal directly from the time-domain by using Parseval's theorem and Fourier transform properties (Hjorth 1970). Several spectral analysis methods (fast Fourier transform, wavelets transform, Wigner-Ville transform, plus many others) can be used to study the frequency contents of the underlying signals. However, Hjorth parameters were chosen because of their low computational cost which makes them favorable for any online data processing task (Khushaba et al. 2014). The description of these parameters starts by first observing Parseval's theorem, which states that the sum of the square of the function is equal to the sum of the square of its transform

$$\sum_{j=0}^{N-1} x[j]^2 = \frac{1}{N} \sum_{k=0}^{N-1} |X[k]X^*[k]| = \sum_{k=0}^{N-1} P[k], \quad (1)$$

where $X[k]$ is the discrete Fourier transform (DFT) of the original signal \mathbf{x} , $P[k]$ is the phase-excluded power spectrum, that is the result of a multiplication of $X[k]$ by its conjugate $X^*[k]$ divided by N , and k is the frequency index. As the complete frequency description derived by the Fourier transform is symmetric with respect to zero frequency (having identical branches stretching into both positive and negative frequencies) (Hjorth 1970), all odd moments will become zero. This is according to the definition of a moment m of order n of the power spectral density of the signal \mathbf{x} which is given by

$$m_n = \sum_{k=0}^{N-1} k^n P[k]. \quad (2)$$

Hjorth parameters are hence mainly based on the lower order even moments, denoted as m_0 , m_2 , and m_4 :

$$m_0 = \sum_{k=0}^{N-1} k^0 P[k] = \sum_{j=0}^{N-1} x[j]^2, \quad (3)$$

$$m_2 = \sum_{k=0}^{N-1} k^2 P[k] = \frac{1}{N} \sum_{k=0}^{N-1} (kX[k])^2 = \frac{1}{N} \sum_{j=0}^{N-1} (\Delta x[j])^2, \quad (4)$$

$$m_4 = \sum_{k=0}^{N-1} k^4 P[k] = \frac{1}{N} \sum_{k=0}^{N-1} (k^2 X[k])^2 = \frac{1}{N} \sum_{j=0}^{N-1} (\Delta^2 x[j])^2, \quad (5)$$

where Δ^n is the n -th derivative of a function in the time-domain, this is according to the time-differentiation property of the Fourier transform. This property states that the power spectrum of a signal in the frequency domain multiplied by k raised to the n -th power is equivalent to n -th derivative of the same signal in the time-domain. Hjorth parameters of interest are then calculated based on the above moments as shown below

$$\text{Activity} = m_0, \quad (6)$$

$$\text{Mobility} = \sqrt{\frac{m_2}{m_0}}, \quad (7)$$

$$\text{Complexity} = \frac{\sqrt{\frac{m_4}{m_2}}}{\text{Mobility}}, \quad (8)$$

Waveform Length (WL):

This is an intuitive measure to describe the cumulative length of the waveform over the considered segment which can also indicate the waveform complexity. The resultant value of the *WL* calculation also indicates a measure of the waveform amplitude, frequency, and duration (Hudgins et al. 1993). For a given hole depth, the *WL* feature value grows larger for signals with higher frequencies than those with lower ones. This is given by

$$WL = \sum_{j=0}^{N-2} |x[j+1] - x[j]|, \quad (9)$$

Simple Square Integral (SSI):

SSI captures the energy of the signal under consideration as a feature (Phinyomark et al. 2010). It can be expressed as

$$SSI = \sum_{j=0}^{N-1} |x[j]|^2, \quad (10)$$

Crest Factor (CF):

CF is defined as the ratio of the absolute value of the peak in the signal under consideration divided by the Root Mean Square (RMS) value of the same signal (Silva 2005). The crest factor indicates how extreme the peaks are in a waveform, with CF of 1 indicating no peaks and larger values indicating more peaks. CF also expresses the size of the dynamic range for an input signal. This is given by

$$CF = \frac{|x_{peak}|}{x_{RMS}}, \quad (11)$$

where

$$x_{RMS} = \sqrt{\frac{1}{N} \sum_{j=0}^{N-1} x[j]^2}, \quad (12)$$

Pressure Ratio (PR):

A new measure was created by taking the ratio of the rotationPressure to that of the feedPressure, this was inspired by the earlier work of Leung and Scheduling (2015). This ratio forms a derived drill performance indicator, the characteristics of which this work attempts to link to the different materials type and chemical assays. These characteristics included all the following:

I summation of the absolute difference between consecutive samples of the PR

- II summation of the PR squared (SPR2) and its logarithmically scaled version
- III summation of the first derivative of the PR squared (SDPR2)
- IV summation of the second derivative of the PR squared (SDDPR2)
- V a logarithmically scaled version of SDPR2/SPR2
- VI a logarithmically scaled version of SDDPR2/SDPR2
- VII the maximum of PR multiplied by the max of *fob*.

Singular-Value Decomposition Entropy (SvdEn):

The dispersion of the singular values λ_k also indicates the complexity of the signal dynamics and is an indicator of how many vectors are needed for an adequate explanation of the signals being studied. To calculate SvdEn, the singular values are first normalized by their total summation

$$\bar{\lambda}_k = \frac{\lambda_k}{\sum \lambda_k}, \quad (13)$$

where $\sum \bar{\lambda}_k = 1$. To denote the dispersion characteristics of the singular values, SvdEn is defined with the Shannon formula applied to the elements of singular values of the matrix and is calculated as shown below (Li et al. 2008).

$$\text{SvdEn} = -\sum \bar{\lambda}_k \log \bar{\lambda}_k, \quad (14)$$

SvdEn can also be considered as a measure of feature-richness in the sense that the higher the entropy of the set of SVD weights, the more orthogonal vectors are required to adequately explain it.

Signal Flatness (F):

This is defined as the ratio between geometric and arithmetic means and is considered as an important measure to distinguish signals that are flat or do not change much, from those that have the amplitude concentrated across small ranges. A high signal flatness (approaching 1.0) indicates that the signal has a similar value across all samples, while a low flatness (approaching 0.0) indicates that the power is concentrated in a relatively small number of samples (Johnston 1988; Dubnov 2004).

$$\text{Flatness} = \frac{\sqrt[N]{\prod_{j=0}^{N-1} x[j]}}{\frac{\sum_{j=0}^{N-1} x[j]}{N}} = \frac{\exp\left(\frac{1}{N} \sum_{j=0}^{N-1} \ln x[j]\right)}{\frac{1}{N} \sum_{j=0}^{N-1} x[j]}, \quad (15)$$

Descriptive Statistics:

The following common statistical measures are also included as features: the signal maximum, standard deviation, skewness, kurtosis, mean, geometric mean, and median of each signal.

3.2 Regression and Classification Models

Several regression and classification models were utilized in this research. The Support Vector Machines (SVM), multivariate Gaussian Process (GP), and Random Forests (RF) models were all utilized for MWD versus assays regression analysis, while

SVMs classification models were also utilized for the detection of the different material-types as described in the experiments section. The details of these models are omitted from this paper as these are traditional algorithms for which the description can be found in general pattern recognition references (Theodoridis and Koutroumbas 2009; Rasmussen and Williams 2005). These models were utilized with the extracted MWD features described in the previous section, with the output of the models being the estimation of the chemical assays for regressions models and the classification labels (material detected or not) for the material detection problem.

The testing scheme utilized with the above models employed a cross-validation process across two modes, these are: (i) random k-fold cross-validation (Stone 1974; 1977) and (ii) spatial k-fold cross-validation (Roberts et al. 2017; Meyer et al. 2019; Talebi et al. 2020). Overall, the goal of cross-validation is to test the model's ability to predict based on new data that was not used for training the models, to flag problems like overfitting or selection bias (Cawley and Talbot 2010), and to give an insight on how the model will generalize to an independent dataset (an unknown dataset). While the cross-validation procedure is the same for random and spatial cross-validation (the process of dividing the data into separate segments for training and testing), the major difference is how the data points are split into folds. The chosen mode of validation is hence largely dependent on the goal of the experiments.

In the case of random k-fold cross-validation, it is generally known that blast-hole sampling is a sparse process, where not all the drilled holes would be considered for logging physical materials or laboratory sampling of chemical assays. In this regard, the general approach is to sample every n -th hole, with n varying across the mine sites depending on design specifications (roughly 1/6 or 1/8 for materials logging and 1/4 for assays sampling). A potential application of this work would be to fill these data gaps with inferred materials and chemical assays, using the nearby holes where data has been recorded as the training set. This mimics the process of random k-fold cross-validation, and the short distance scales do not require spatial k-fold cross-validation for this demonstration. The random k-fold cross-validation experiments are included as a proxy for this use case.

In the case of spatial k-fold cross-validation, recent literature has shown that when using a model trained on spatial data to make inferences on data collected from a spatially distant environment, the commonly used random cross-validation may provide considerably over-optimistic error estimates due to the problem of spatial autocorrelation (Roberts et al. 2017; Meyer et al. 2018). Cross-validation strategies based on random data splitting fail to assess models' performance in terms of spatial mapping. If the objective is to test the model's performance upon spatially distant datasets, then a spatially-aware cross-validation scheme will provide more realistic outcomes to accurately estimate the generalization errors. In this regard, we have implemented a leave-one-blast-out scheme of testing in which the data from all holes belonging to a specific blast is kept away for testing, while the remaining data from all other blasts are used for training (a process that is repeated across all blasts). This mimics the use-case of predicting assays in a new blast in real-time from MWD data, before assays and material logs take place, or for selected blasts where these are not economically viable.

For most of the regression models, Bland-Altman graphs and QQ-plots are shown to verify the outcome of these models in comparison to the laboratory measurements. To verify the results statistically, the following measures are also shown on the correlation graphs:

- I **eq** - slope and intercept equation
- II **r** - Pearson r-value
- III **RMSE** - root mean squared error
- IV **p** - Pearson correlation p -value
- V **n** - number of data points used
- VI **RPC** - reproducibility coefficient ($1.96 \cdot SD$)
- VII **CV** - coefficient of variation (SD of mean values in %)

The Bland-Altman plot is presented as a scatter plot in which the x-axis represents the average of a pair of measurements $(A + B)/2$, and the y-axis shows the difference between the two paired measurements $(A - B)$. The Bland-Altman plot allows visual inspection for several aspects of the comparability of outcomes of the utilized model against the actual laboratory measurements. First, a consistent measure of bias can be described. This is the mean of all the differences between the algorithms' outcomes and the laboratory measurements. This mean is represented as a line across the x-axis of the plot, with the difference between this value and y-values describing the magnitude and direction of the bias. Bias can be reported in absolute terms or as a percentage (bias/mean value). The Bland-Altman plots are also utilized to study any proportional bias between the model outcomes and the laboratory measurements. The existence of proportional bias indicates that the model and laboratory measurements do not agree equally through the range of measurements (the limits of the agreement will depend on the actual measurement).

4 Experimental Results

In this section, the feasibility of predicting several assays from MWD data with the various regression models is investigated. The proposed approach is demonstrated on selected assay types, as a general proof of concept. The results in the following sections are acquired using the random k-fold cross-validation mode (as filling in the gaps was the primary motivator of this research), unless otherwise specified that the spatially-aware cross-validation mode was used.

4.1 Iron (Fe) Prediction

The regression results for predicting iron (Fe) using GP, SVM, and RF models are shown in Fig. 3 and Fig. 4 for Regions A and B respectively. For Region A, both SVM and GP had a Pearson correlation coefficient of 0.79 with the laboratory readings for Fe, with an RMSE of 2.7 and 2.8 respectively for GP and SVM. RF performed similarly to GP and SVM, with a correlation coefficient of 0.78 and an RMSE value of 2.8. For Region B, both GP and SVM again performed similarly, though with a

lower Pearson correlation coefficient of 0.64, and RMSE of 5.4, while RF achieved a correlation coefficient of 0.63, and RMSE of 5.4. All regression models from both sites had p -values less than 0.001, which indicates a significant correlation between the Fe estimates from these models vs. that from the corresponding laboratory measurements. From these results, it is clear that all models achieved better results on Region A data in comparison to the performance on Region B. Therefore, further analysis to understand the differences between Regions A and B were carried out.

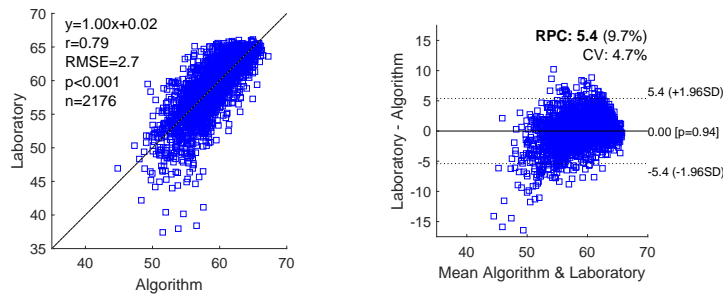
The distributions of the laboratory measurements of Fe from both sites were then studied to understand the differences between Regions A and B. Fig. 5 shows the QQ-plot for both sites individually against the quantiles of normal distribution, and also against each other's quantiles. The results in Fig. 5 clearly demonstrate that Fe samples from each site are not normally distributed and that the samples of Region A Fe do not come from the same distribution as Region B Fe. Further evidence that these distributions are different is seen in the histogram of the Fe samples from each site, as shown in Fig. 6. Both histograms are skewed, but Region B Fe exhibits twice the kurtosis of Region A Fe.

As the performance of these models on the Fe data was similar across both mining sites, the estimates generated by the SVM models were selected for further analysis. The histogram of the residuals, that is the difference between laboratory Fe measurements and SVM Fe estimations, are shown in Fig. 7. These histograms clearly indicate that the majority of Region A samples had a difference between laboratory and estimated values of ± 2.5 , which is the typical tolerance in the assay error for Fe and SiO_2 as indicated in the literature (Wedge et al. 2018). However, the Region B residuals were concentrated around ± 5 . It is important to note here that the tolerances are usually set independently for each element and may vary from project to project, according to requirements or the interval's iron grade, as less accurate validation is required for low-grade (waste) intervals. In general, low Fe values of $\text{Fe} < 50$ are classified into waste, while $50 \leq \text{Fe} < 60$ are classified as med-grade and $\text{Fe} \geq 60$ are classified as high-grade. When plotting the residuals across these three classes of Fe grades, it was observed that the tail of the histograms in Fig. 6 with large negative values were all related to low-grade iron as shown in Fig. 8. These larger errors occur well under the waste cut-off, so are unimportant as the exact Fe content will not be considered in further decision-making at such low values.

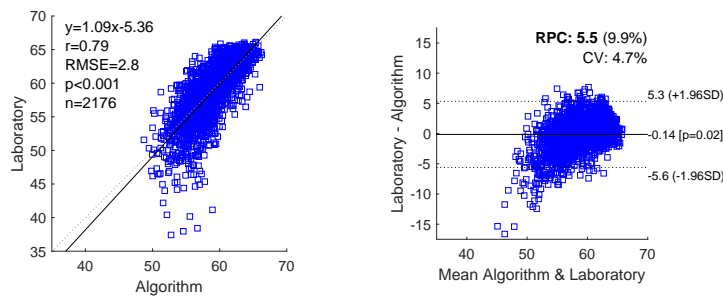
4.2 Phosphorus (P) Prediction

In these experiments, the two datasets from Region A and Region B were combined to generate one large set of samples, as each site contains a relatively small number of samples. The results in Fig. 9 demonstrate the performance of the machine learning models in predicting P values from the MWD data. In this case, the RF model demonstrated the highest correlation with the laboratory measurements of 0.81, with an RMSE of 0.03. The GP model had a correlation coefficient of 0.79, and SVM of 0.78, both with an RMSE of 0.03.

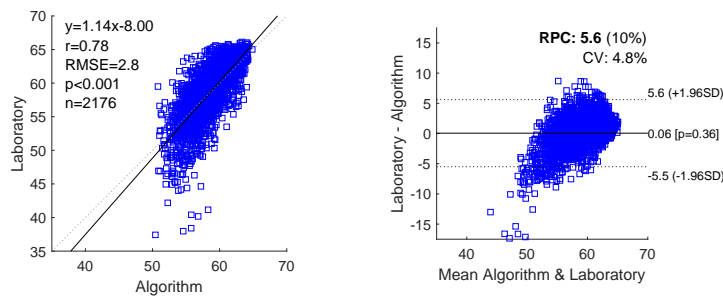
In order to understand more about what impacted these correlation values, we plotted the difference between the laboratory P measurements and RF predictions of



(a) GP model results



(b) SVM model results



(c) RF model results

Fig. 3 Region A Bland-Altman iron (Fe) regression plots with several models

P versus the laboratory P measurements. In this way, one can clearly see where the laboratory and model disagree, and observe the actual range of P across the corresponding samples. The results in Fig. 10 clearly show that very few of the approximately 4000 samples had a measured P value > 0.35, and these were essentially ‘missed’ by the model, as the model did not observe sufficient samples of this magnitude to learn the relationship between MWD and P across that range. Hence, the

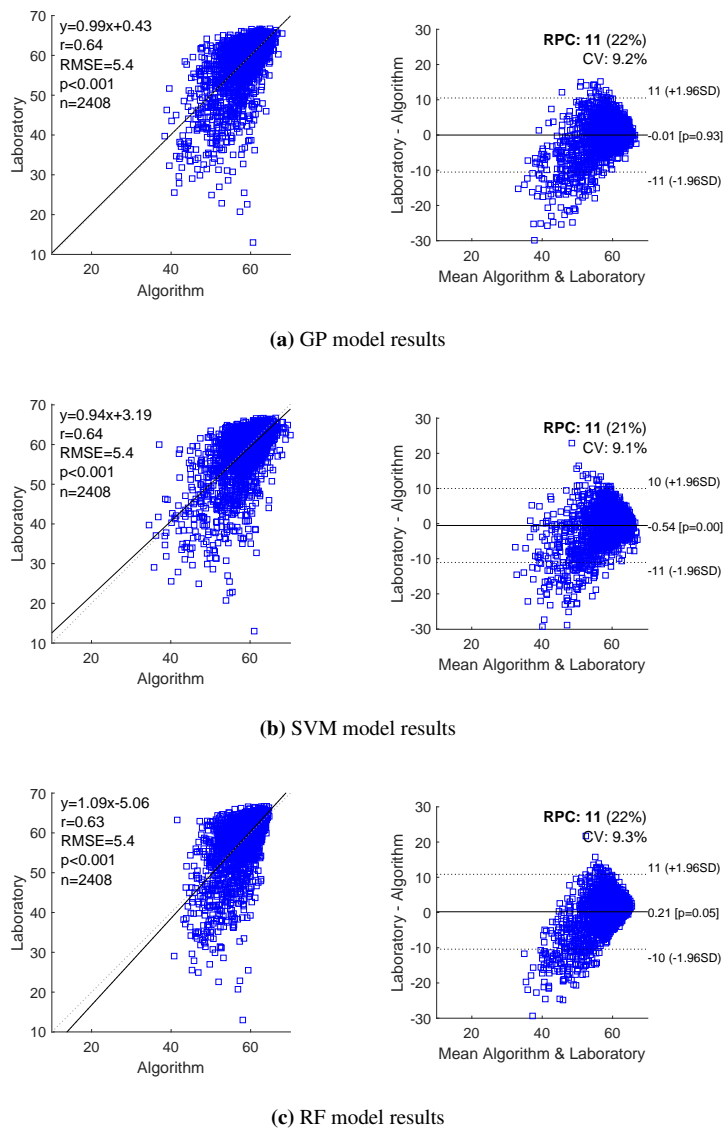


Fig. 4 Region B Bland-Altman iron (Fe) regression plots with several models

sample size available for this experiment did impact the accuracy of estimation. It is believed that having much larger datasets with a significantly larger number of samples would enhance the models' performance. Considering the available samples, the performance of the models with an RMSE of 0.03 is quite promising, given that the literature has no previously reported figures in this regard, to the best of the authors' knowledge.

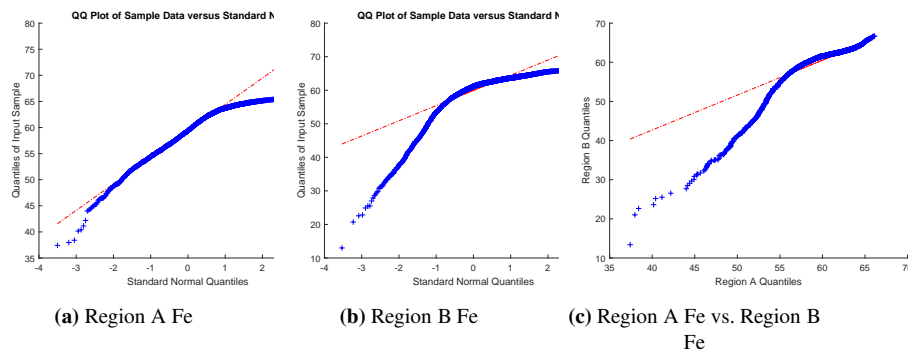


Fig. 5 QQ-plots displaying empirical quantile-quantile plot for Regions A and B. Samples from both mining sites are not normally distributed, and both samples do not come from the same distribution

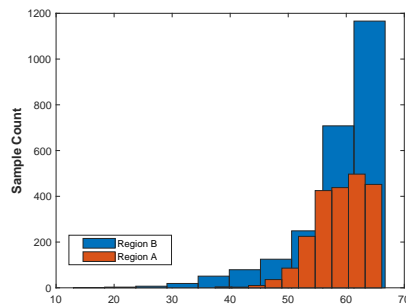


Fig. 6 Histogram of Fe samples from Regions A and B showing clear differences in distributions between the two mining sites

4.3 Sulfur (S) Prediction

The results for predicting S based on the combined MWD data from Regions A and B are shown in Fig. 11 using the GP, SVM, and RF models. These results clearly demonstrate that the accuracy of the proposed approach generally depends on the assay type (for example, Fe, P, S, etc.) and distribution within the two mining sites, with Sulfur having correlation coefficients as high as 0.91 using GP model with an RMSE of 0.0027. On the other hand, the raw measurements of S and their GP predictions based on MWD data are also shown in Fig. 12, which further visually demonstrates the effectiveness of the method proposed in this paper.

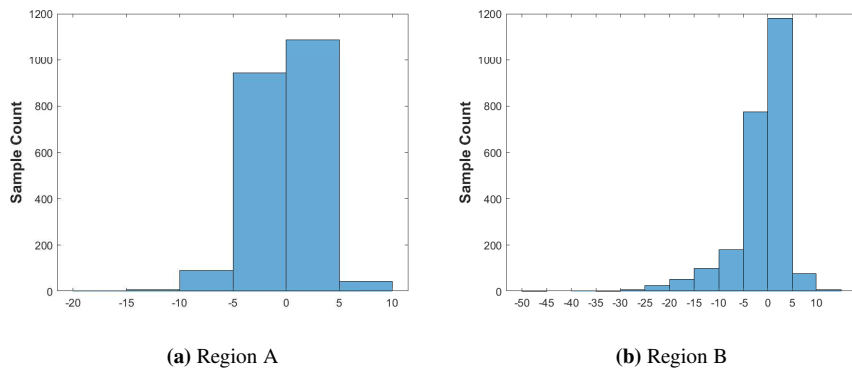


Fig. 7 Histogram of the difference between laboratory Fe and SVM estimation of Fe on Regions A and B samples

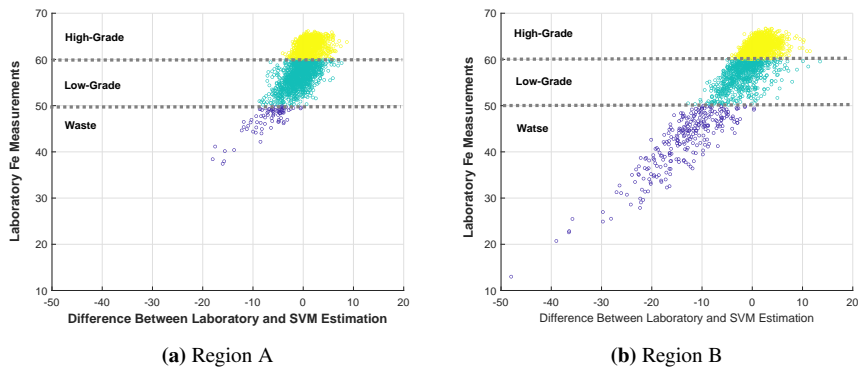
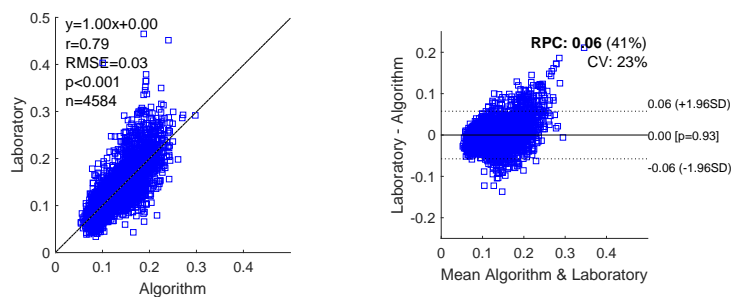


Fig. 8 The difference between laboratory Fe and SVM estimation of Fe against the classifications of Fe into low, med and high-grades, on Regions A and B samples

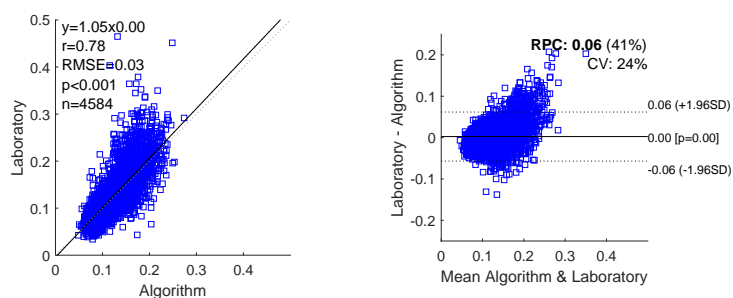
4.4 Spatially-Aware Cross-Validation

In order to develop a spatially-aware cross-validation scheme, we first plot the spatial distribution of the available blast-holes across the patterns from the two mining sites of Region A and Region B as shown in Fig. 13. Our spatial cross-validation process involved a leave-one-blast-out process, in which all of the holes related to an individual blast are kept for testing while training is based on the data from all other holes from all remaining blasts. The process is repeated across each of the blasts to ensure that the testing is performed across all of the blasts in the data set. Performance estimates are computed based on the final results to validate the overall assay estimation performance across spatially different blasts.

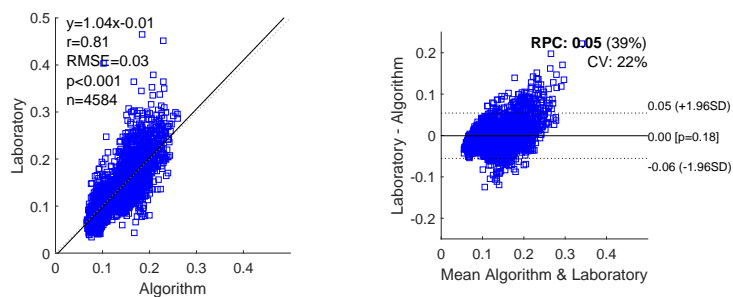
The spatially-aware regression results for both P and S are shown in Fig.14 using an RF model. These results demonstrate that the model's performance when estimat-



(a) GP model results



(b) SVM model results



(c) RF model results

Fig. 9 Combined Phosphorus (P) data, Regions A and B, Bland-Altman regression plots with several machine learning models

ing these two chemical assays using a spatially-aware mode significantly dropped in comparison to the previously demonstrated P and S results when using random k-fold cross-validation. This is in line with the literature findings in that, in the random k-fold cross-validation mode, autocorrelation could have impacted the results. Given the purpose of our first experiment was to fill in the missing gaps of chemical

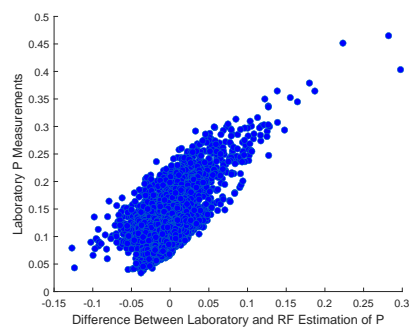


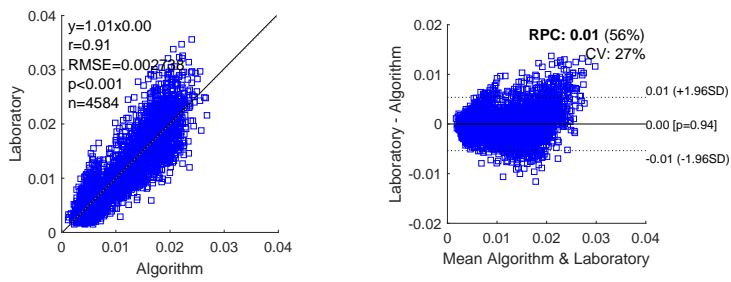
Fig. 10 Difference between laboratory measurements and RF estimation of P vs. laboratory P measurements

assays for blast-holes, the previous performance measures are advantageous within the context and objective of this first testing scheme. In comparison, the results of the spatially-aware cross-validation scheme could have been impacted by several factors including first, the limited size of the available data, with only 4584 samples across both sites, and second, the different distributions of the assays across the two sites. Hence, the authors conclude that further experimentation with a significantly larger dataset would be required to properly judge the modelling accuracy of assays from MWD across spatially distance locations.

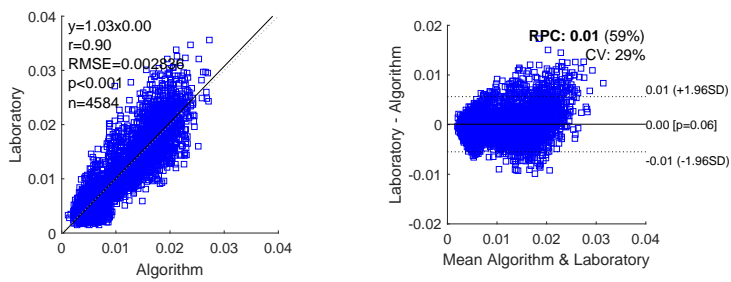
4.5 Cross-Assay Predictions

The goal of this experiment is to verify whether the knowledge about one assay type can better inform the models about the distributions of other assays, that is to indicate if, for example, the knowledge of Fe or SiO₂ can inform Al₂O₃, or other such assay combinations. For this specific test, the RF model was selected as an example of the available regressions models, as the performance is similar across GP, SVM and RF, and the purpose is simply to demonstrate the concept. The experiment proceeded by first analyzing whether there is any correlation between the different assays, which is shown to be the case in Fig. 15. The results for predicting Al₂O₃ using MWD alone, MWD together with Fe, and MWD together with SiO₂ are each shown in Fig. 16. These results show significant enhancements to Al₂O₃ accuracy (correlation and RMSE) when using the combination of MWD with one additional chemistry assay. This supports the hypothesis that knowing one assay type can significantly enhance the prediction performance for other assay types. The benefit of this finding is that if one assays type can be measured or predicted with some sensor/model, then these measurements can be used to improve estimates for other assays, a subject of future investigation.

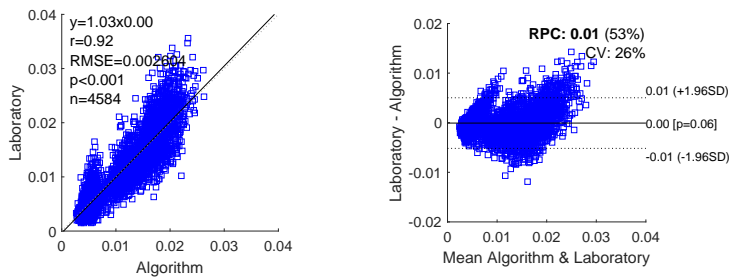
The analysis also included a spatially-aware cross-validation test on cross-assay prediction. In this regard, the results for predicting Al₂O₃ using MWD together with Fe, and MWD together with SiO₂ are shown in Fig. 17. It is evident from these



(a) GP model results



(b) SVM model results



(c) RF model results

Fig. 11 Combined Sulfur (S) data, Regions A and B, Bland-Altman regression plots with several machine learning models

results that the correlation coefficients dropped in comparison to those obtained by the same models with a random cross-validation scheme, which indicates the impact of autocorrelation in this case. However, these results are also encouraging as the spatially-aware models' performance can be largely enhanced by knowing the distribution of other assays estimates. For example, the same approach can be used with

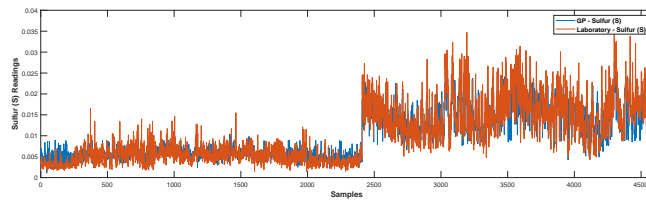
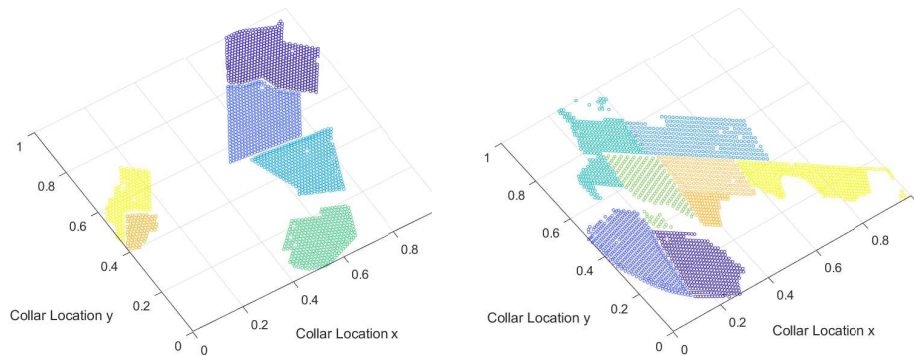


Fig. 12 Raw Sulfur (S) laboratory and GP model predictions showing high agreement between measurements and predictions



(a) Region A blast-hole distribution

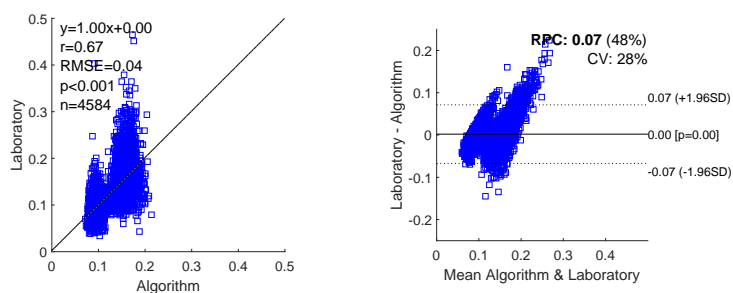
(b) Region B blast-hole distribution

Fig. 13 Spatial distribution of the blast-holes across the two sites, with colors representing the different blasts across the two sites. The x-y coordinates have been re-scaled due to commercial sensitivity

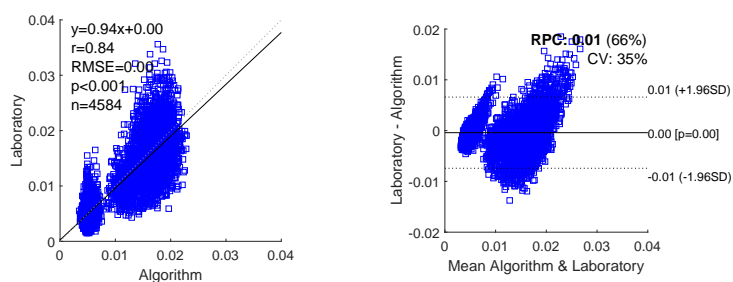
a technology relying on PFTNA that estimates most assays apart from P, in order to estimate these missing P values. Combining MWD with a selection of PFTNA-estimated assays to fill in the missing chemistry values warrants further investigation.

4.6 Multivariate vs. Univariate Response Predictors

While the main aim of this paper was to prove the concept of assay and material prediction via machine learning models, it could be argued that using machine learning approaches to predict multivariate response values are now available (for example, multivariate random forests) (Segal and Xiao 2011), and thus the univariate prediction of assay grades is a limited step forward. To validate the effectiveness of the multivariate RF response predictor against the traditional univariate version, a comparison between both models was performed to predict all assays types. The results in Fig. 18 show no significant differences in terms of the correlation coefficients between the two multivariate and univariate RF models, except for Mn, which could be



(a) Phosphorus (P) regression results



(b) Sulfur (S) regression results

Fig. 14 Spatially-aware regression results for Phosphorus (P) and Sulfur (S) using individual RF models

due to the limited data size and the distribution of the data from the two sites. However, it is important to note that the multivariate version predicted all responses in one step. In a real-time system deployment, this may translate to a significant reduction in the computational requirements associated with building several individual chemistry assay predictors. For offline predictions, it appears both multivariate and univariate approaches are suitable.

4.7 Material Type Classification

In this section, an experiment employing SVM as a classifier to predict the presence or absence of different material-types was conducted. The purpose is to estimate whether or not a given percentage of the material under consideration is present at the specified location. This is a process for which the threshold utilized to define the existence/absence of a certain material can vary from one material type to another, as different materials may become operationally relevant at different proportions. For the purpose of this paper, as we are primarily interested in a proof of concept, a

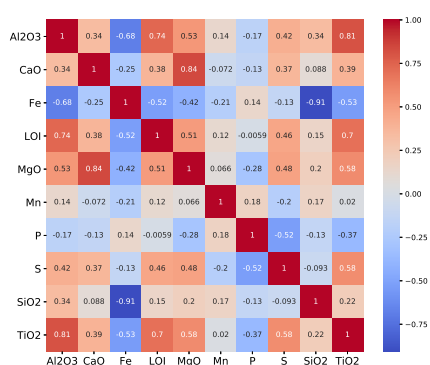


Fig. 15 Pearson correlation coefficients among all assays from both mining sites

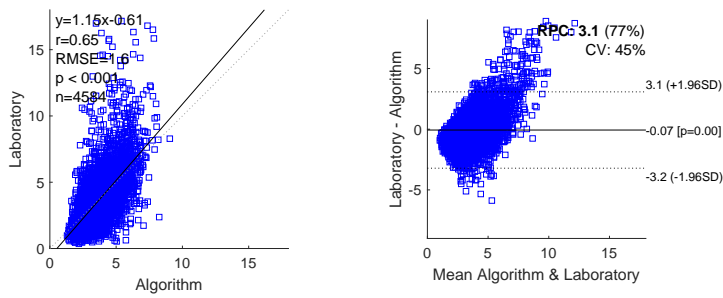
threshold of 0% was selected; any value greater than zero is taken to indicate the presence of the material under investigation. The SVM model is well suited to this analysis as SVM models were originally developed for binary classification problems such as this one.

Eight material-types were randomly selected from all existing material types, in no specific order, to demonstrate the feasibility of this concept. The results for this section are shown in Fig. 19 for the following material types: i) shale (SHL), ii) banded iron formation (BIF), iii) powdery banded iron formation (BPO), iv) goethite ochreous (GOL), v) hematite goethite medium (HGM), vi) hematite goethite friable (HGF), vii) shale ferruginous (SHF), and viii) goethite martite vitreous goethite matrix (GMO). Given the available number of samples, these results demonstrate that MWD can be used to predict the presence/absence of different material-types with accuracies in the order of 80–90% across the selected material types.

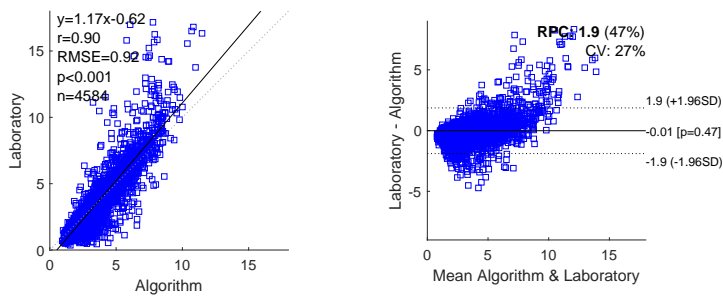
4.8 Feature Importance and Selection

The importance of the various features used for assay prediction is compared in this section, to provide insights into the different features' relevance for this application. This is aided by algorithms such as RF providing a measure of predictor importance for process discovery analysis.

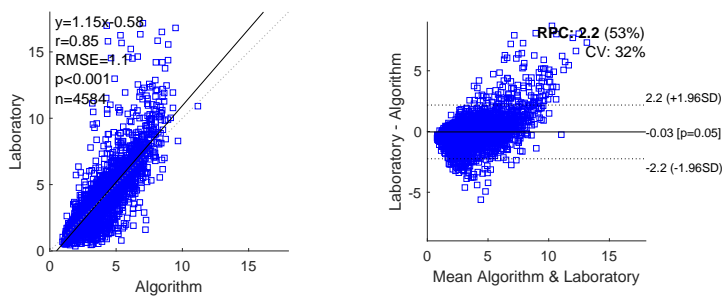
In this case, the analysis showed that the top ten features that were highly ranked by RF for Fe predictions in Region A included i) the maximum values of torque, rotationPressure, and pressure ratio, ii) the waveform length of rotationPressure and pressure ratio, iii) the standard deviation of pressure ratio, iv) Hjorth activity of pressure ratio, torque, and sed, and v) median of airPressure. For predicting Fe in Region B, the following features were ranked as top ten by the utilized RF model, including i) the flatness of sed and rop, ii) Hjorth activity of sed, iii) Hjorth mobility and complexity of rop, iv) standard deviation of sed and rop, v) median of airPressure and rotationPressure, and vi) kurtosis of rop. For Sulfur prediction across the combined data from the two regions, the top ten features included all of i) the median of rop,



(a) RF model results predicting Al_2O_3 using MWD only



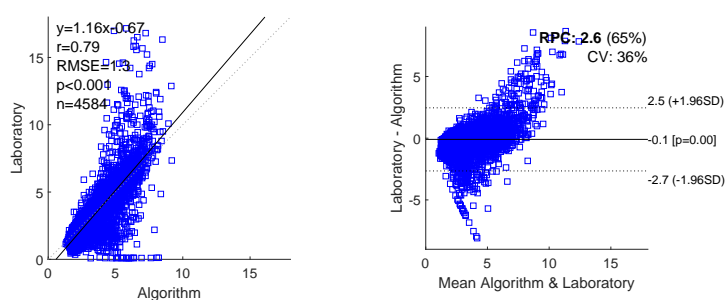
(b) RF model results predicting Al_2O_3 using MWD with Fe



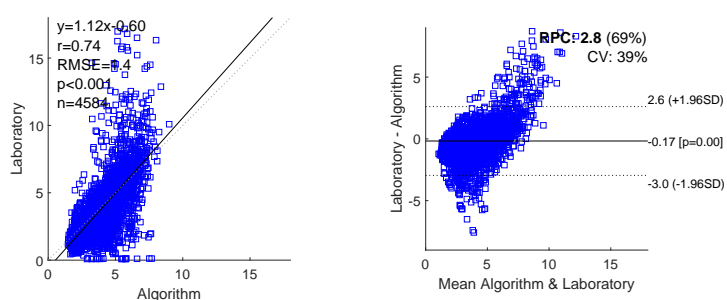
(c) RF model results predicting Al_2O_3 using MWD with SiO_2 .

Fig. 16 The impact of combining MWD with other individual chemistry assays to predict Al_2O_3

airPressure, torque and sed, ii) Hjorth activity of airPressure, rop, torque and sed, and iii) geometric mean of rop, airPressure. On the other hand, for predicting phosphorus based on the combined data from two regions, the utilized RF model ranked the top features to include i) geometric mean of rop and airPressure, ii) median of rop air-



(a) RF model results predicting Al_2O_3 using MWD with Fe from a spatially-aware cross-validation scheme



(b) RF model results predicting Al_2O_3 using MWD with SiO_2 from a spatially-aware cross-validation scheme

Fig. 17 Spatially-aware cross-validation test on cross-assay prediction

Pressure and rotationRPM, iii) Hjorth activity of airPressure, rop, and sed, iv) Hjorth complexity of sed, and v) the integral sum of rotationRPM.

As can be seen from the above list of features, the ranking and the type of top ten contributing features to each assay estimation accuracy would be different from one chemical assay to another and could be even different from one region to another (depending on the distribution of the data and the amount of available data). In the context of the available data within this study, Hjorth parameters (specifically the activity), waveform length, flatness and basic statistics were almost always among the top-ranked features. This does not exclude the importance of the remaining features but is simply intended to highlight the common key features. As the primary goal of this paper was to prove the feasibility of predicting assays and materials from MWD data, a more thorough analysis of the feature importance and ranking will be included in future work on a larger dataset.

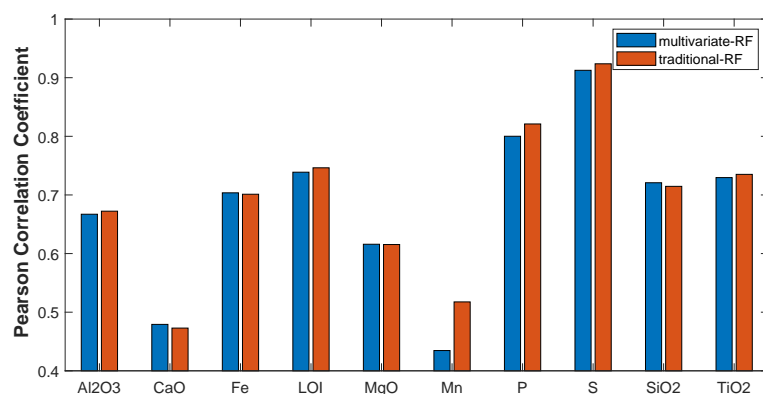


Fig. 18 Multivariate vs. univariate RF response predictors

5 Discussion

The results presented in this paper indicate that the approach of mapping MWD to materials types and chemical assay values is feasible, leading to the conclusion that machine learning algorithms can be employed to predict materials and assays. While this was only demonstrated on eight materials types, the findings do generalize across a broader set of materials (excluded for brevity). It is important to mention here that our findings also suggest that the accuracy of this mapping process is primarily dependent on (i) assay/material type and its distribution across the mining sites from which the data was acquired and (ii) the amount of available data. It was also found that the choice of the regression model, among GP, SVM and RF models, did not significantly alter the findings, as the quality of the estimation performed by these machine learning models mainly depended on the quality of the extracted features.

The analysis started with Fe estimation using GP, SVM, and RF models, with results suggesting that Fe estimation across Region A was more accurate than that across Region B. The distribution of Fe across the two mining sites was then examined in Fig. 6 and it was found that the two mining sites had significantly different distributions of iron as the histogram of Fe across Region B spiked much higher than that across Region A (larger kurtosis value). This in turn explains part of the variability of the results from both sites. Further variability appears to come from limitations on the available data, with approximately 2000 samples available for each site resulting in fewer samples within some classes (waste, low-grade, high-grade). It is important to note that the largest Fe prediction errors were actually made within the waste class, as was shown in Fig. 8, while much more consistent predictions were made along low-grade and high-grade iron where the predicted values would actually be relevant.

In terms of Phosphorus (P), the largest prediction errors were made along values larger than 0.35, as when combining data from Regions A and B it was found that out of the set of nearly 4000 samples, only around 11 Phosphorus samples were avail-

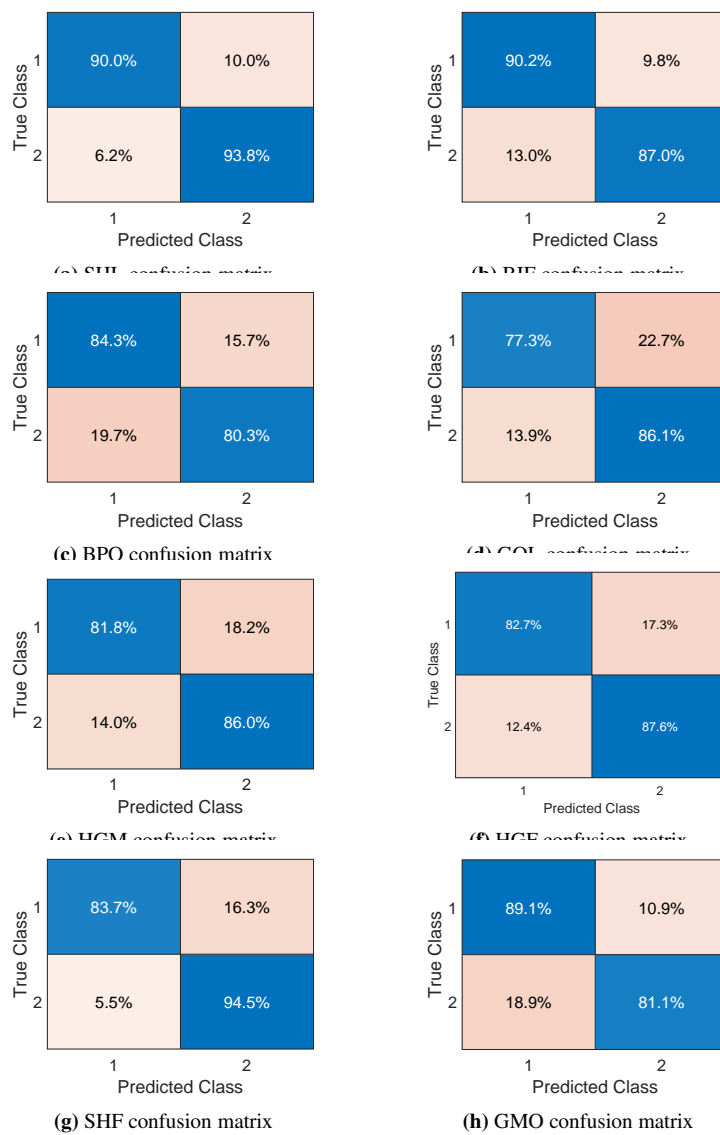


Fig. 19 Classification confusion matrices to inform us about the accuracy with which one can identify the existence of different material-types: 1 - Material does not exist, 2 - Material exist

able with values larger than 0.35. Hence, there was not enough data for the GP, SVM and RF models to learn the relationship between MWD and high Phosphorus values. However, the overall prediction accuracy of Phosphorus suggests its estimation is useful, with a Pearson correlation coefficient of 0.81, RMSE of 0.3, and a p -value of < 0.001 . This indicates significant correlations between laboratory measurements

and estimations by our models. In terms of Sulfur (S), the predictions shown in this paper were found to be most accurate when combining the data from the two mining sites, with the best results achieved by RF with a correlation coefficient of 0.92, RMSE of 0.002604, and a p -value of < 0.001 .

The effectiveness of using knowledge about one assay type to assist the prediction of other assays was investigated. The hypothesis, in this case, is that if one algorithm or sensor can predict one assay type accurately, then one can make use of this knowledge to better predict other assays. For this part of the analysis, when using the MWD features with an RF model, the combined Regions A and B data had a correlation coefficient of 0.65 with an RMSE of 1.6 when predicting Al_2O_3 . However, these results were significantly enhanced by adding either Fe ($r = 0.9$, $\text{RMSE} = 0.92$) or SiO_2 ($r = 0.85$, $\text{RMSE} = 1.1$), as was shown in Fig. 16. The reason for selecting these two assays to augment MWD data when predicting Al_2O_3 is that high correlations were observed between these assays, as depicted in Fig. 15. Hence, the knowledge of either of these assays supported the model to more accurately estimate the Al_2O_3 values.

In the final part of the experiments, we presented a proof of concept that MWD can also predict the presence or absence of material types. Eight different materials types including i) SHL, ii) BIF, iii) BPO, iv) GOL, v) HGM, vi) HGF, vii) SHF and viii) GMO were randomly selected to demonstrate this. The confusion matrices generated when using the SVM as a classifier to predict material presence or absence showed, in general, accuracies over 80% achieved with the available data.

6 Conclusion

In this paper, a proof of concept has been presented for using machine learning and MWD data to predict the presence or absence of material types and estimate chemical assay values. It is important to note that while different applications of MWD have been previously considered in the literature, the study presented in this paper is the first to use MWD for material logging and assaying purposes, to the best of the authors' knowledge. The findings of this study strongly support the feasibility of the proposed approach, with results showing correlations between MWD features and assays types of up to 0.92 for individual assays. The analysis has also shown that the accuracy depends on the distribution of the data and the assay type being predicted. It was also demonstrated that the presence or absence of material types can be predicted while drilling by using MWD data based on a limited dataset.

The findings of this paper are important to the mining industry as the timeliness and quality of these estimations cascade through the downstream mining processes. Knowledge of material-types and chemical assays can play a significant role in mining, guiding the drilling process, orebody modeling, and providing chemistry data with down-hole resolution. The generated predictions and estimates of material types and assays can also further help guide mine planning. The work in this field continues as the authors plan to investigate the impact of using deep learning models on much larger datasets from a wider range of sites. Further studies will be conducted on automatic feature extraction in comparison to the handcrafted feature extraction approach

utilized in this paper, which demonstrated the feasibility of using this MWD data for logging and assaying.

Acknowledgements This work has been supported by the Australian Centre for Field Robotics and the Rio Tinto Centre for Mine Automation. The authors would also like to acknowledge the support of Anna Chlingaryan and Katherine Silversides in the manuscript review and editing process.

References

- Box J, Phillips J, Clout J (2002) Use of geological material types for predicting iron ore product characteristics. FUWA – Ward Iron and Steel Making Workshop
- Cawley G, Talbot N (2010) On over-fitting in model selection and subsequent selection bias in performance evaluation. *Journal of Machine Learning Research* 11:2079–2107
- Clark I, Dominy S (2017) Underground bulk sampling, uniform conditioning and conditional simulation - unrealistic expectations? Eighth World Conference on Sampling and Blending :61
- Dubnov S (2004) Generalization of spectral flatness measure for non-gaussian linear processes. *Signal Processing Letters, IEEE* 11:698 – 701
- Galende M, Menéndez M, Fuente M, Sainz-Palmero G (2018) Monitor-while-drilling-based estimation of rock mass rating with computational intelligence: The case of tunnel excavation front. *Automation in Construction* 93:325–338
- Hatherly P, Leung R, Scheduling S, Robinson D (2015) Drill monitoring results reveal geological conditions in blasthole drilling. *International Journal of Rock Mechanics and Mining Sciences* 78:144–154
- Hjorth B (1970) Eeg analysis based on time domain properties. *Electroencephalography and Clinical Neurophysiology* 29(3):306 – 310, ISSN 0013-4694
- Hudgins B, Parker P, Scott R (1993) A new strategy for multifunction myoelectric control. *IEEE transactions on bio-medical engineering* 40:82–94
- Jeanneau P, Flahaut V, Maddever R (2017) Iron ore benefits from neutron pulsed geochemical tools. Conference proceedings: IRON ORE 2017, Perth, Australia) 2017:387–396
- Johnston J D (1988) Transform coding of audio signals using perceptual noise criteria. *IEEE Journal on Selected Areas in Communications* 6(2):314–323
- Khanal M, Qin J, Shen B, Dlamini B (2020) Preliminary investigation into measurement while drilling as a means to characterize the coalmine roof. *Resources* 9:10
- Khorzoughi M, Hall R, Apel D (2018) Rock fracture density characterization using measurement while drilling (mwd) techniques. *International Journal of Mining Science and Technology* 28:504–516
- Khushaba R N, Takruri M, Miro J V, Kodagoda S (2014) Towards limb position invariant myoelectric pattern recognition using time-dependent spectral features. *Neural Networks* 55:42 – 58, ISSN 0893-6080
- Leung R, Scheduling S (2015) Automated coal seam detection using a modulated specific energy measure in a monitor-while-drilling context. *International Journal of Rock Mechanics and Mining Sciences* 75:196–209, ISSN 1365-1609
- L'Heureux A, Grolinger K, Elyamany H F, Capretz M A M (2017) Machine learning with big data: Challenges and approaches. *IEEE Access* 5:7776–7797
- Li S y, Yang M, Li C c, Cai P (2008) Analysis of heart rate variability based on singular value decomposition entropy. *Journal of Shanghai University (English Edition)* 12:433–437
- Market J, Byrne C, Robinson D, Jeanneau P, Rossiter H (2019) Downhole assays in the pilbara. Conference proceedings: IRON ORE 2019, Perth, Australia) 2019:366–386
- McHugh C, Stokes A, Oppolzer F, Rogers B (2012) Automated multi-drills in rio tinto. Conference proceedings: Proceedings Eighth Open Pit Operators' Conference , (The Australasian Institute of Mining and Metallurgy: Melbourne) 2012:83–88
- Meyer H, Reudenbach C, Hengl T, Katurji M, Nauss T (2018) Improving performance of spatio-temporal machine learning models using forward feature selection and target-oriented validation. *Environmental Modelling and Software* 101:1–9, ISSN 1364-8152
- Meyer H, Reudenbach C, Wöllauer S, Nauss T (2019) Importance of spatial predictor variable selection in machine learning applications – moving from data reproduction to spatial prediction. *Ecological Modelling* 411:108815, ISSN 0304-3800

- Navarro J, Sanchidrián J, Segarra P, Castedo R, Costamagna E, López L (2018) Detection of potential overbreak zones in tunnel blasting from mwd data. *Tunnelling and Underground Space Technology* 82:504–516
- Paine M, Boyle C, Lewan A, Phuak E, Mackenzie P, Ryan E (2016) Geometallurgy at rtio – a new angle on an old concept. *Third AusIMM International Geometallurgy Conference* :55–61
- Park J, Kim K (2020) Use of drilling performance to improve rock-breakage efficiencies: A part of mine-to-mill optimization studies in a hard-rock mine. *International Journal of Mining Science and Technology* 30(2):179–188, ISSN 2095-2686
- Phinyomark A, Hirunviriyaya S, Limsakul C, Phukpattaranont P (2010) Evaluation of emg feature extraction for hand movement recognition based on euclidean distance and standard deviation. *International Conference on Electrical Engineering/Electronics Computer Telecommunications and Information Technology (ECTI-CON)*, Chiang Mai 2010:856 – 860
- Rai P, Schunesson H, Lindqvist P A, Kumar U (2015) An overview on measurement-while-drilling technique and its scope in excavation industry. *Journal of The Institution of Engineers (India): Series D* 96:57–66
- Rasmussen C E, Williams C K I (2005) *Gaussian Processes for Machine Learning (Adaptive Computation and Machine Learning)*. The MIT Press, ISBN 026218253X
- Roberts D R, Bahn V, Ciuti S, Boyce M S, Elith J, Guillera-Arroita G, Hauenstein S, Lahoz-Monfort J J, Schröder B, Thuiller W, Warton D I, Wintle B A, Hartig F, Dormann C F (2017) Cross-validation strategies for data with temporal, spatial, hierarchical, or phylogenetic structure. *Ecography* 40(8):913–929
- Segal M, Xiao Y (2011) Multivariate random forests. *WIREs Data Mining and Knowledge Discovery* 1(1):80–87
- Silva C (2005) *Vibration and Shock Handbook*
- Silversides K L, Melkumyan A (2020) Boundary identification and surface updates using mwd. *Mathematical Geosciences* :1–25
- Smith C, Jeanneau P, Maddever R, Fraser S, Rojc A, Lofgren M, Flahau V (2015) PFTNA logging tools and their contributions to in-situ elemental analysis of mineral boreholes. *TOS forum* 5:157 – 165
- Sommerville B, Boyle C, Brajkovich N, Savory P, Latscha A A (2014) Mineral resource estimation of the brockman 4 iron ore deposit in the pilbara region. *Applied Earth Science* 123(2):135–145
- Stone M (1974) Cross-validatory choice and assessment of statistical predictions. *Journal of the Royal Statistical Society: Series B (Methodological)* 36(2):111–133
- Stone M (1977) An asymptotic equivalence of choice of model by cross-validation and akaike's criterion. *Journal of the Royal Statistical Society Series B (Methodological)* 39(1):44–47, ISSN 00359246
- Talebi H, Peeters L, Mueller U, Tolosana-Delgado R, Van den Boogaart K (2020) Towards geostatistical learning for the geosciences: A case study in improving the spatial awareness of spectral clustering. *Mathematical Geosciences* 52
- Theodoridis S, Koutroumbas K (2009) *Pattern Recognition*. ISBN 978-1-59749-272-0
- Wedge D, Hartley O, McMickan A, Green T, Holden E J (2019) Machine learning assisted geological interpretation of drillhole data: Examples from the pilbara region, western australia. *Ore Geology Reviews* 114:103118, ISSN 0169-1368
- Wedge D, Lewan A, Paine M, Holden E J, Green T (2018) A data mining approach to validating drill hole logging data in pilbara iron ore exploration. *Economic Geology* 113:961–972
- Zhou H, Monteiro S, Hatherly P, Ramos F, Nettleton E, Oppolzer F (2010) Automated rock recognition with wavelet feature space projection and gaussian process classification. *Proceedings - IEEE International Conference on Robotics and Automation* :4444–4450